

Metals versus Non-metals: Chemical Evolution of Hydrogen and Helium Isotopes in the Milky Way

JAMES W. JOHNSON,¹ MIQUELA K. WELLER,^{2,3} AND RYAN J. COOKE^{4,5}

¹*Carnegie Science Observatories, 813 Santa Barbara St., Pasadena, CA 91101, USA*

²*Department of Astronomy, The Ohio State University, 140 W. 18th Ave., Columbus, OH 43210, USA*

³*Center for Cosmology & AstroParticle Physics (CCAPP), The Ohio State University, 191 W. Woodruff Ave., Columbus, OH 43210, USA*

⁴*Centre for Extragalactic Astronomy, Durham University, Durham, DH1 3LE, UK*

⁵*Department of Physics, Durham University, South Road, Durham DH1 3LE, UK*

ABSTRACT

Star formation drives changes in the compositions of galaxies, fusing H and He into heavier nuclei. This paper investigates the differences in abundance evolution between metal and non-metal isotopes using recent models of Galactic chemical evolution appropriate for the thin disk epoch. A strong degeneracy arises between metal yields from stellar populations and the mean Galactocentric radial velocity of the interstellar medium (ISM). Similar metallicities arise when increases (decreases) in metal yields are combined with increases (decreases) to the gas flow velocity. A similar degeneracy exists between metal yields and the rate of gas ejection from the ISM. We demonstrate that this degeneracy can be confidently broken with precise measurements of the hydrogen (D/H) and helium ($^3\text{He}/^4\text{He}$) isotope ratios in the Galactic ISM. At fixed O/H, higher metal yields lead to higher D/H and lower $^3\text{He}/^4\text{He}$. Measurements available to date are not sufficiently precise or numerous to draw confident conclusions. A detailed inventory of non-metal isotopes in the Milky Way would provide critical empirical constraints for stellar and galactic astrophysics, as well as a new test of Big Bang Nucleosynthesis. We forecast that only \sim 4 additional measurements of $^3\text{He}/^4\text{He}$ within \sim 3 kpc of the Sun are required to measure the primordial $^3\text{He}/^4\text{He}$ ratio at \sim 30% precision. In parallel, empirical benchmarks on metal yields also have the power to inform stellar models, since absolute yield calculations carry factor of \sim 2 – 3 uncertainties related to various complex processes (e.g., rotational mixing, convection, mass loss, failed supernovae).

1. INTRODUCTION

The chemical compositions of gas and stars encode a wealth of information on the assembly and evolution of their host galaxies. The information in these measurements is often interpreted through the lens of Galactic chemical evolution (GCE) models (see discussion in, e.g., the reviews by [Tinsley 1980](#) and [Matteucci 2021](#)). However, these models are affected by uncertainties in key quantities. In particular, the total mass of metals produced by stellar populations is difficult to constrain empirically (see discussion in, e.g., [Weinberg et al. 2024](#)). This metal production factor, or “yield,” is degenerate with the amount of mass that gets ejected from the interstellar medium (ISM; e.g., [Sandford et al. 2024](#)). In this paper, we show that GCE models incorporating radial gas flows (e.g., [Lacey & Fall 1985](#); [Biliewski & Schönrich 2012](#)) are affected by a similar degeneracy. We further demonstrate that abundance measurements of non-metal isotopes in the interstellar medium would not only break this degeneracy, but also provide useful constraints for stellar evolution and a new test of current models of Big Bang Nucleosynthesis (BBN; see, e.g., the seminal works by [Alpher et al. 1948](#); [Hoyle & Tayler 1964](#); [Peebles 1966](#); [Wagoner et al. 1967](#), and the more

recent reviews by [Schramm & Turner 1998](#); [Steigman 2007](#); [Cooke 2024](#)).

Stellar models do not confidently predict metal yields. Poorly understood processes, such as mass loss (e.g., [Sukhbold et al. 2016](#)), convection and convective boundaries (e.g., [Chieffi et al. 2001](#); [Ventura et al. 2013](#)), and nuclear reaction rates (e.g., [Herwig & Austin 2004](#); [Herwig 2005](#); [Kotar et al. 2025](#)), introduce uncertainties of a factor of a \sim few in the mass of metals released to the ISM at the end of a star’s life (see discussion in, e.g., [Johnson et al. 2023b](#) in the context of nitrogen). This paper highlights prior work demonstrating similar effects due to rotation ([Limongi & Chieffi 2018](#)) and black hole formation ([Griffith et al. 2021](#)) in high mass stars (see discussion in Section 5.1 below). This uncertainty is problematic for GCE models, since stellar yields play a direct role in establishing metal abundances. Previous GCE models with sufficiently large yields often incorporate ejection, which lowers metallicity by removing metals from the ISM and replacing them with hydrogen gained through accretion (see discussion in, e.g., [Weinberg et al. 2017](#)). This connection results in a classic “source-sink” degeneracy, whereby metals can be more efficiently produced but also more efficiently ejected, resulting in similar present-day abundances

(e.g., Hartwick 1976; Cooke et al. 2022; Johnson et al. 2023c; Sandford et al. 2024).

Stellar yields are also difficult to constrain empirically. One method, perhaps the most direct, would be to simply count up all of the metals and all of the stars in the local Universe (e.g., Prochaska et al. 2003; Gallazzi et al. 2008; Peebles et al. 2014; see also the review by Péroux & Howk 2020). However, this approach requires reliable measurements of the metallicities of circumgalactic media (CGM; Tumlinson et al. 2017). The CGM metallicity varies substantially both between and within individual halos, making it difficult to pin down mass-weighted averages (e.g., Zahedy et al. 2019, 2021; Cooper et al. 2021; Haislmaier et al. 2021; Kumar et al. 2024; Sameer et al. 2024). Overall metal abundances are also subject to uncertainties in abundance determination (see, e.g., the review by Kewley et al. 2019).

A second diagnostic of the scale of stellar yields comes from observing supernovae (SNe) themselves. Rodríguez et al. (2023) measured the mean Fe yield of Type II SNe by examining the radioactive tails of their lightcurves. Weinberg et al. (2024) extended their measurement to infer population-averaged yields, which quantify the metal mass produced per unit mass of star formation. In addition to the statistical uncertainty itself, their inference is also affected by systematic uncertainties in the number of SNe that arise from a stellar population of a given mass (e.g., Pejcha & Thompson 2015; Ertl et al. 2016; Sukhbold et al. 2016). The ratio of α -capture and iron-peak element yields from massive stars is also an important source of uncertainty with this method (see discussion in Sit et al. 2025).

A third diagnostic of stellar yields is rooted in trends in metallicity with stellar age. The efficient ejection, coupled with efficient metal production to maintain abundances at plausible levels, has a secondary effect on enrichment timescales, which in turn influences age-metallicity trends. In Johnson et al. (2025), we focused on the recent empirical result that stellar metallicities exhibit a remarkably flat trend with age (e.g., Spina et al. 2022; da Silva et al. 2023; Willett et al. 2023; Gallart et al. 2024). Across much of the Galactic disk, metallicity declines by only ~ 0.1 dex between ages of $\tau \sim 0$ and ~ 10 Gyr (Roberts et al. 2025). Our models in Johnson et al. (2025) reproduced this flat trend more readily if stars make \sim twice as many metals as inferred by Weinberg et al. (2024). The required level of metal production is smaller if accreting gas is pre-enriched to low metallicity (see discussion in Johnson et al. 2025) or if the rates of all SNe are higher at low metallicity (e.g., Gandhi et al. 2022; Pessi et al. 2023; Johnson et al. 2023a). Nuance regarding these processes makes it challenging to pin down the scale of yields using stellar ages, which are notoriously difficult to measure as well (e.g., Soderblom 2010; Chaplin & Miglio 2013).

Each of these diagnostics of metal production are affected by their own sources of systematic uncertainty. In light of these challenges, this paper advocates that the community dedicate effort to an additional approach. In particular, we show that this degeneracy between stellar yields, the rate of ejection, and the radial gas velocity can be broken using precise measurements of the isotope ratios of non-metals. The data products would not only break this fundamental degeneracy in GCE models, but also enable the first estimate of the primordial helium isotope ratio, $(^3\text{He}/^4\text{He})_p$.

This paper is organized as follows. We describe $^3\text{He}/^4\text{He}$ and D/H measurements presently available in the literature in Section 2 below. We describe our GCE models in Section 3. We illustrate the yield-ejection-velocity degeneracy and demonstrate that it can be broken with D/H and $^3\text{He}/^4\text{He}$ in Section 4. We discuss techniques for measuring non-metal isotope ratios and the potential impact of the data products in Section 5. We conclude in Section 6.

2. DATA

We use measurements of $^3\text{He}/^4\text{He}$ and D/H available in the literature. Mahaffy et al. (1998) measured both isotope ratios in Jupiter's atmosphere using data from the Galileo Probe Mass Spectrometer (Niemann et al. 1992). These measurements can be attributed to the composition of the protosolar nebula. We also use measurements of D/H in the local ISM compiled by Linsky et al. (2006), which are drawn from prior work available at the time (see references therein).

Additional measurements of $^3\text{He}/^4\text{He}$ in the Milky Way (MW) have been reported by Balser & Bania (2018) and Cooke et al. (2022). Cooke et al. (2022) measured $^3\text{He}/^4\text{He}$ along the line of sight toward a hot massive star in the Orion Nebula, $\Theta^2\text{A}$ Ori (O'Dell et al. 1993), using a combination of optical and infrared transitions ($\lambda 3188$ Å, $\lambda 3889$ Å, and $\lambda 1.0833$ μm) of metastable helium, He^1 . Balser & Bania (2018) measured $^3\text{He}^+/\text{H}^+$ and $^4\text{He}^+/\text{H}^+$ in five Galactic H II regions using spin-flip transitions and radio recombination lines in the 8 – 10 GHz frequency range using the Green Bank Telescope. We omit one of these H II regions (Sh 2-209) because its distance is unclear. The Balser & Bania (2018) catalog lists a Galactocentric radius of $R = 16.2$ kpc, but Yasui et al. (2023) found $R = 10.3$ kpc based on near-infrared imaging and astrometric data from Gaia EDR3 (Gaia Collaboration et al. 2021). The helium isotope ratio of Sh 2-209 is $^3\text{He}/^4\text{He} = (1.41 \pm 0.28) \times 10^{-4}$, which is consistent with our adopted primordial ratio (see Section 3.1.2 below). A Galactocentric radius of $R = 10.3$ kpc would therefore place this H II region slightly but not significantly below the rest of the Balser & Bania (2018) sample (see Figure 2 below).

3. GALACTIC CHEMICAL EVOLUTION MODELS

We use multi-zone GCE models from Johnson et al. (2025) and Johnson (2025). Specifically, we use the parameter

choices that are broadly consistent with the equilibrium scenario for the MW. We integrate these models numerically using the publicly available VERSATILE INTEGRATOR FOR CHEMICAL EVOLUTION (VICE; Johnson & Weinberg 2020)¹. In this class of GCE models, the ISM metallicity rapidly approaches some steady-state, after which increases in the overall abundance are negligible (see also Larson 1972 and Weinberg et al. 2017). Johnson et al. (2025) demonstrated that this type of enrichment history reproduces trends in metallicity with stellar population age much more accurately than models predicting larger increases in abundances during the thin disk epoch. We adopt our models directly from Johnson et al. (2025) and Johnson (2025), making no modifications with the exception of including helium and deuterium in the VICE integrations.

These models discretize the Galactic disk into $\delta R = 100$ pc rings between $R = 0$ and 20 kpc, capturing the effects of enrichment in different regions of the MW. Each annulus is coupled to its nearest neighbors through the exchange of gas and stellar populations, but enrichment is otherwise described by a conventional “one-zone” GCE model where stellar yields mix instantaneously and homogeneously with the star forming ISM (see, e.g., the reviews by Tinsley 1980 and Matteucci 2021). We determine the present-day Galactocentric radius of each stellar population by sampling from a normal distribution centered on the radius of formation. The width of the distribution, and by extension the distances stars have migrated, increases with population age. The Galaxy follows the observed Kennicutt-Schmidt relation (Schmidt 1959, 1963; Kennicutt 1998), wherein the surface densities of gas and star formation follow a single power-law relation, $\dot{\Sigma}_\star \propto \Sigma_g^N$, with $N = 1.5$.

Each annulus follows a star formation history (SFH) that initially rises rapidly before falling for the remainder of the disk lifetime, according to

$$\dot{\Sigma}_\star \propto \left(1 - e^{-t/\tau_{\text{rise}}}\right) e^{-t/\tau_{\text{sfh}}}. \quad (1)$$

In each of our models, the values of τ_{rise} and τ_{sfh} increase with Galactocentric radius such that the models reproduce the observed profile in stellar age. The exact prescription for τ_{rise} and τ_{sfh} differs slightly between our ejection- and flow-driven models, but the differences are unimportant to this paper. The radial flow models from Johnson (2025) use pure exponential scalings in τ_{rise} and τ_{sfh} with scale lengths of $r_{\text{rise}} = 6.5$ kpc and $r_{\text{sfh}} = 4.7$ kpc, respectively. Our ejection-driven models from Johnson et al. (2025) use a piece-wise prescription that nonetheless closely resembles this simple exponential. These prescriptions encode the “inside-out” nature of disk

formation, wherein the inner regions assemble first on short timescales followed by the outer regions on longer timescales (see discussion in, e.g., Bird et al. 2013).

3.1. Stellar Yields

Motivated by uncertainties in the overall scale of stellar yields (see discussion in Section 1), we follow two assumed normalizations in this paper. The first follows the recommendation by Weinberg et al. (2024) based on the determination of the mean Fe yield from the radioactive tails of Type II SN lightcurves by Rodríguez et al. (2023). The mass fraction of a given stellar population’s initial mass later released to the ISM in a given element is approximately equal to its solar abundance by mass. We refer to this overall yield scale as $y/Z_\odot = 1$. Our second normalization is a factor of two larger, so we refer to this assumption as $y/Z_\odot = 2$.

The yields of D, ^3He , and ^4He are significantly more well-understood than metal production. We discuss how we accommodate non-metals at the different scales individually. ^3He and ^4He have significant contributions from asymptotic giant branch (AGB) stars. VICE handles this enrichment channel by determining the total mass of dying stars from all timesteps leading up to the current time according to

$$\dot{\Sigma}_x^{\text{AGB}} = \int_0^t y_x^{\text{AGB}}(M_{\text{TO}}, Z) \dot{\Sigma}_\star(t') h(t - t') dt', \quad (2)$$

where h describes the fraction of a single stellar population’s mass that is in the form of main sequence stars at a given age. VICE determines $h(t)$ based on a specified initial mass function, for which we use the Kroupa (2001) form in this work, and a stellar mass-lifetime relation, for which we use the Larson (1974) form. The yield, y_x^{AGB} , is evaluated at the main sequence turnoff mass, M_{TO} , and metallicity of stellar populations at each previous timestep, integrated up to the current time, t . Further details on the implementation of AGB star yields in VICE can be found in Johnson & Weinberg (2020) and Johnson et al. (2023b).

3.1.1. Oxygen

We focus on O as the representative metal in this paper. Stellar populations release oxygen on timescales much shorter than the dynamical time of the Galactic disk, and O is commonly measured in the gas-phase, making it a useful diagnostic for both theoretical and observational purposes. Oxygen makes up 0.572% of the mass of the Sun based on the photospheric abundance measurements by Asplund et al. (2009). A hypothetical 1000 M_\odot stellar population would therefore produce 5.72 M_\odot of O under the $y/Z_\odot = 1$ normalization. Newly produced O appears in the ISM immediately after star formation, an approximation justified by the short lifetimes of massive stars relative to the age of the Galactic disk (e.g., Maeder & Meynet 1989; Padovani & Matteucci 1993; Hurley

¹ Install: <https://pypi.org/project/vice>. Documentation: <https://vice-astro.readthedocs.io>. Source Code: <https://github.com/giganano/VICE.git>.

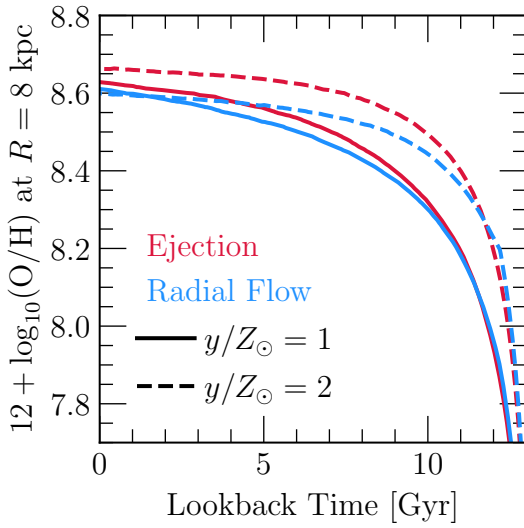


Figure 1. Evolution of the ISM O abundance with time at $R = 8$ kpc in our four GCE models. Models using ejection of ISM gas from the disk versus those using radial flows within the disk (see discussion in Section 3.2) are color coded red and blue, respectively. Models using the $y/Z_{\odot} = 1$ scale of stellar yields versus those using $y/Z_{\odot} = 2$ (see discussion in Section 3.1) are marked as solid and dashed lines, respectively. **Summary:** Models enrich on different timescales depending on the scale of metal yields but otherwise lead to the same O/H abundances in the ISM at the present day.

et al. 2000). We clarify that Weinberg et al. (2024) used the Magg et al. (2022) solar composition, but their calculations ultimately constrain the scale of stellar yields relative to the solar abundance as opposed to the absolute yield.

3.1.2. Helium

Weller et al. (2025) investigated which prescriptions for ${}^4\text{He}$ yields reproduce observed trends between ${}^4\text{He}$ and O abundances. Based on their recommendations, we use a linear relation between the total ${}^4\text{He}$ yield, the O yield, and the solar abundances of O and He (see their equation 12). Following Cooke et al. (2022), we use the yields of ${}^3\text{He}$ and ${}^4\text{He}$ from AGB stars calculated by Lagarde et al. (2011, 2012). We determine population-averaged yields of ${}^3\text{He}$ and ${}^4\text{He}$ by calculating the total mass released to the ISM after a stellar population has evolved for 10 Gyr. We adopt a massive star ${}^4\text{He}$ yield that makes up the difference between the AGB yield and the total inferred by Weller et al. (2025). Weller et al. (2025, in preparation) make further recommendations for ${}^3\text{He}$ yields based on ${}^3\text{He}$ abundance measurements available in the literature. The massive star yield of ${}^3\text{He}$ is subdominant, so production of this isotope is driven by AGB star yields anyway. Following Cooke et al. (2022), we use the non-rotating massive star ${}^3\text{He}$ yields from Limongi & Chieffi (2018).

We retain the primordial ${}^3\text{He}$ and ${}^4\text{He}$ abundances from Cooke et al. (2022). Our primordial helium abundance

(by mass) is $Y_{\text{P}} = 0.24721$ based on Pitrou et al. (2021), and our primordial helium isotope ratio (by number) is ${}^3\text{He}/{}^4\text{He} = 1.257 \times 10^{-4}$. For both ${}^3\text{He}/{}^4\text{He}$ and D/H, adjusting the primordial composition simply shifts the predicted isotope ratios up or down uniformly across the Galaxy, so the exact choice is not particularly important for our purposes. However, we note that the primordial ${}^3\text{He}/{}^4\text{He}$ has never been directly measured, while the primordial D/H has (see discussion below and in Section 5.2).

3.1.3. Deuterium

The evolution of D is arguably the simplest of all atomic nuclei. Protostars are fully convective, which eventually draws all deuterium nuclei into layers hot enough to fuse them into helium (Bodenheimer 1966; Mazzitelli & Moretti 1980). Consequently, all D nuclei that are incorporated into stars should be destroyed. We therefore set all D yields to zero and shut off the return of D to the ISM from stellar envelopes in VICE. The notion that stars both synthesize metals and destroy deuterium leads to a direct one-to-one relationship between metallicity and D/H (Weinberg 2017; van de Voort et al. 2018). We use a primordial D abundance of $(\text{D/H})_{\text{P}} = 2.53 \times 10^{-5}$ from Cooke et al. (2018) in this paper.

3.2. Ejection versus Radial Gas Flows

3.2.1. Ejection-Driven Models

Our models adopted from Johnson et al. (2025) incorporate ejection from the ISM due to feedback. The mass-loading factor, $\eta \equiv \dot{\Sigma}_{\text{wind}}/\dot{\Sigma}_{\star}$, describes the mass ejected due to Galactic winds per unit mass of star formation (see discussion in, e.g., the reviews by Veilleux et al. 2020 and Thompson & Heckman 2024). These models use an exponential scaling with Galactocentric radius,

$$\eta = \eta_{\odot} e^{(R-R_{\odot})/r_{\eta}}, \quad (3)$$

where $R_{\odot} = 8$ kpc is the location of the Sun (e.g., GRAVITY Collaboration et al. 2019). The observed metallicity gradient in the Galactic disk reflects the observed gradient if $r_{\eta} = 7$ kpc, with $\eta_{\odot} = 0.4$ for $y/Z_{\odot} = 1$ and $\eta_{\odot} = 1.4$ for $y/Z_{\odot} = 2$ (Johnson et al. 2025).

3.2.2. Radial Gas Flow-Driven Models

Our models in Johnson (2025) use the inward flow of gas toward the Galactic center (e.g., Lacey & Fall 1985; Portinari & Chiosi 2000; Spitoni & Matteucci 2011; Bilitewski & Schönrich 2012; Pezzulli & Fraternali 2016). We examined several prescriptions for the radial velocity of the ISM, finding that equilibrium chemical evolution arises when the flow speed is relatively constant in both radius and time. Based on our analytic models therein, we use $v_{r,g} = -0.5$ km/s and -1.8 km/s as the velocities associated with the $y/Z_{\odot} = 1$ and 2 yield scales, respectively. These models include a weak,

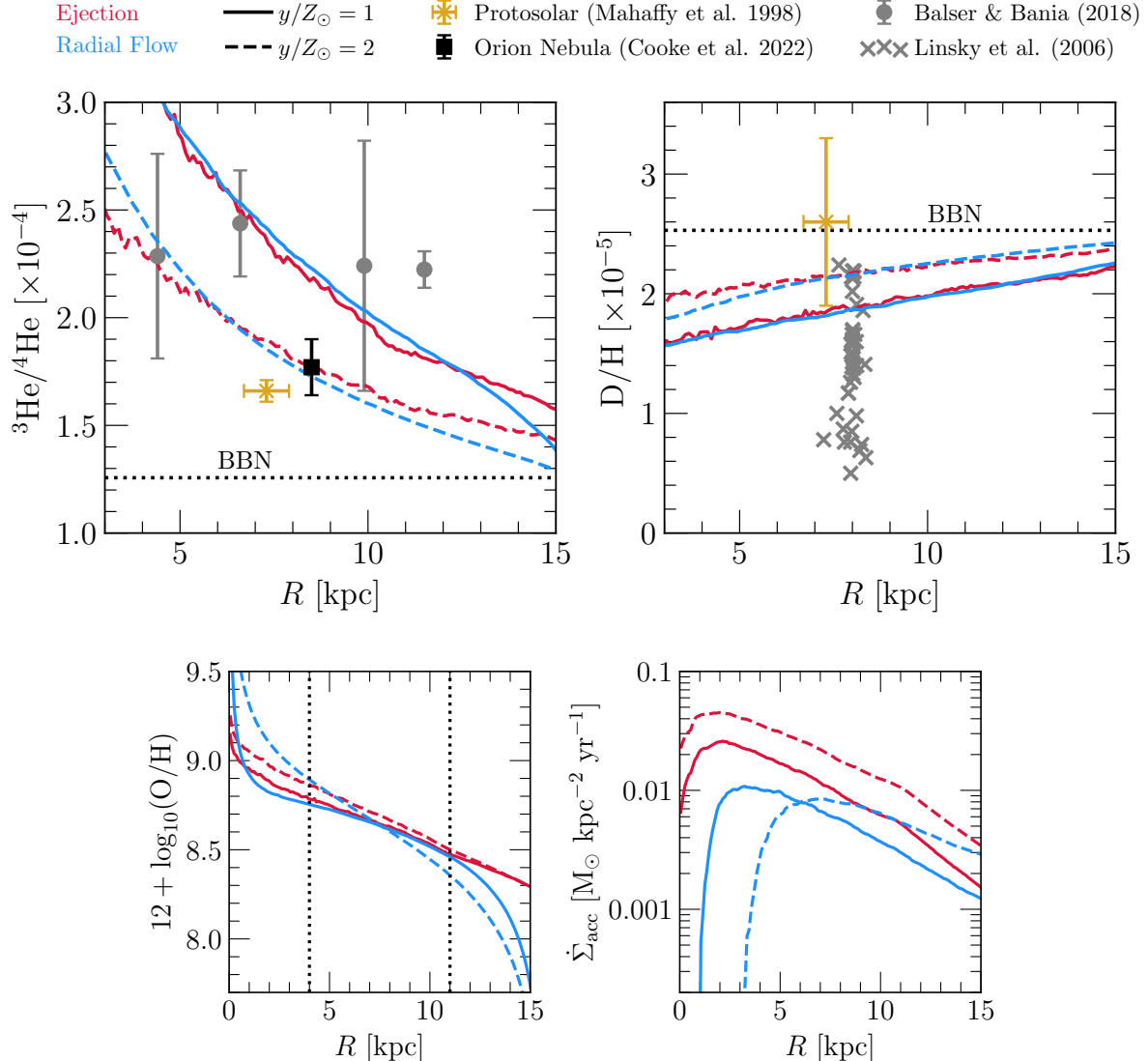


Figure 2. Present day radial profiles of the ${}^3\text{He}/{}^4\text{He}$ and D/H ratios (top), the O abundance (bottom left), and the surface density of gravitational accretion (bottom right). Top panels show measurements of the non-metal isotope ratios available in the literature (see discussion in Section 2). The lower left panel highlights the $R \sim 4 - 11$ kpc range as the region of the MW where these data reside. **Summary:** Overall, our GCE models have similar profiles in metallicity, but different yield scales lead to different normalizations in the D/H and ${}^3\text{He}/{}^4\text{He}$ profiles.

centrally concentrated ejection process in order to counteract the pile-up of material in the inner Galaxy (see discussion in Johnson 2025). This prescription satisfies only this criterion, with $\eta_{\odot} = 0.2$ and $r_{\eta} = -5$ kpc, which leaves ejection sufficiently weak across much of the disk that the radial flow is a much more dominant effect on chemical enrichment.

4. THE DEGENERACY

Figure 1 shows the evolution in the O abundance at $R = 8$ kpc over time in our GCE models at the two scales of stellar yields that we consider. The predicted evolution traces the yield scale much more closely than the choice of ejection or radial gas flows. The present-day ISM metallicities of

each model are not distinguishable empirically, indicating that present-day gas-phase abundance measurements cannot confidently discriminate between yield scales. Others have quantified the degeneracy between yields and ejection rates in the past (e.g., Hartwick 1976; Cooke et al. 2022; Johnson et al. 2023c; Sandford et al. 2024). Here, we find a similar relationship between the yield and the ISM radial velocity. This comparison also indicates that it would be difficult to empirically distinguish the effects of ejection from radial gas flows. Johnson (2025) discusses this topic in the context of metal abundances.

In light of Figure 1, one possible means with which to break this degeneracy is by comparing the metal abundances

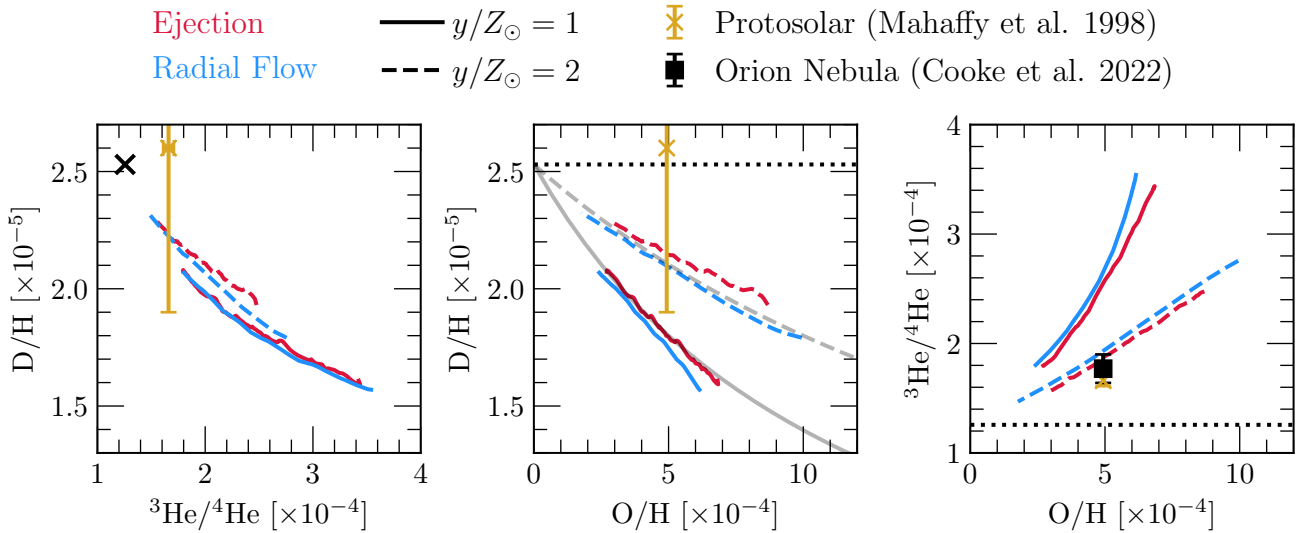


Figure 3. The relationship between O/H, D/H, and ${}^3\text{He}/{}^4\text{He}$. Each panel shows the relationship between a pair of two quantities traced by the present-day ISM between $R = 3$ and 12 kpc. Lines are colored and styled based on the GCE model with yield scales $y/Z_\odot = 1$ or 2 (solid or dashed) and adopting ejection or radial gas flows (red or blue). Our adopted primordial isotope ratios (see Section 3.1) are shown as a black \times in the left panel and black dotted lines in the middle and right panels. At present, the Sun is the only astrophysical system with a measurement in all three of these panels, though the measurement corresponds to the protosolar composition as opposed to the present day (Mahaffy et al. 1998). Grey lines in the middle panel show the D/H-O/H relation computed by Weinberg (2017) for $y/Z_\odot = 1$ (solid) and $y/Z_\odot = 2$ (dashed). The black square in the right panel shows our measurement of the ${}^3\text{He}/{}^4\text{He}$ ratio in the Orion Nebula (Cooke et al. 2022) assuming solar metallicity (e.g., D’Orazi et al. 2009). **Summary:** This three-way relationship between O/H, D/H, and ${}^3\text{He}/{}^4\text{He}$ can provide measurements of both the scale of stellar yields and the primordial D/H and ${}^3\text{He}/{}^4\text{He}$ ratios simultaneously.

in stars with their ages. Distinguishing between the $y/Z_\odot = 1$ and $y/Z_\odot = 2$ scenarios requires an abundance precision of $\ll 0.2$ dex in ~ 10 Gyr old populations. Modern spectroscopic surveys achieve statistical uncertainties in α -capture and iron-peak elements at this level (e.g., APOGEE, Majewski et al. 2017; SDSS-V Milky Way Mapper, Mészáros et al. 2025; GALAH, Buder et al. 2025). However, abundances vary systematically between surveys at the ~ 0.1 dex level (e.g., Griffith et al. 2022; Hegedűs et al. 2023). Stellar age measurements are also substantially challenging, especially for old populations (see the reviews by, e.g., Soderblom 2010 and Chaplin & Miglio 2013). In Johnson et al. (2025), we discussed how the strikingly flat nature of the observed age-metallicity relation tentatively favors the $y/Z_\odot = 2$ scale. However, a $y/Z_\odot = 1$ model can achieve good agreement with the data by incorporating either pre-enriched accretion from the CGM or metallicity-dependent supernova rates (see discussion in Section 1). Breaking this yield-ejection-velocity degeneracy with this approach is therefore not without substantial nuance in model parameterizations, compounding the issues from measurement uncertainties.

Figure 2 demonstrates how this degeneracy can be broken using the ${}^3\text{He}/{}^4\text{He}$ and the D/H ratios in the ISM. By construction, each model predicts similar O abundance profiles in the $R \approx 4 - 11$ kpc range, where our models are most applicable to the MW (see discussion in, e.g., Johnson et al.

2021). However, the ${}^3\text{He}/{}^4\text{He}$ and D/H profiles follow noticeably different normalizations. With high yields, the high rates of ejection are accompanied by high rates of accretion, which introduces metal-poor gas to the local ISM. A similar effect arises with radial gas flows, with the main difference being that the more metal-poor material comes from larger radii in the Galactic disk as opposed to the CGM. By definition, this more metal-poor gas mixing with the local ISM is closer to the primordial composition. D/H and ${}^3\text{He}/{}^4\text{He}$ both reflect these effects similarly. We note that the radial flow model predicts lower accretion rates overall than the ejection model. This difference arises because ejection necessitates additional accretion in order to reach the stellar mass of the MW, whereas radial gas flows are not allowed to change the total mass of the ISM (Johnson 2025).

In line with our investigation of age-metallicity trends in Johnson et al. (2025), the helium isotope ratio of the Orion Nebula seems to favor the $y/Z_\odot = 2$ scale of stellar yields. The protosolar ${}^3\text{He}/{}^4\text{He}$ (Mahaffy et al. 1998) is slightly below the model in the local ISM, but we have verified that the two are consistent in the snapshot 4.6 Gyr ago. The protosolar D/H, however, is not measured with sufficient precision for our purposes, nor are the ${}^3\text{He}/{}^4\text{He}$ measurements in the radio (Balser & Bania 2018). The Linsky et al. (2006) D/H sample exhibits substantial scatter, which they interpreted as a consequence of deuterium depletion onto dust grains. If this

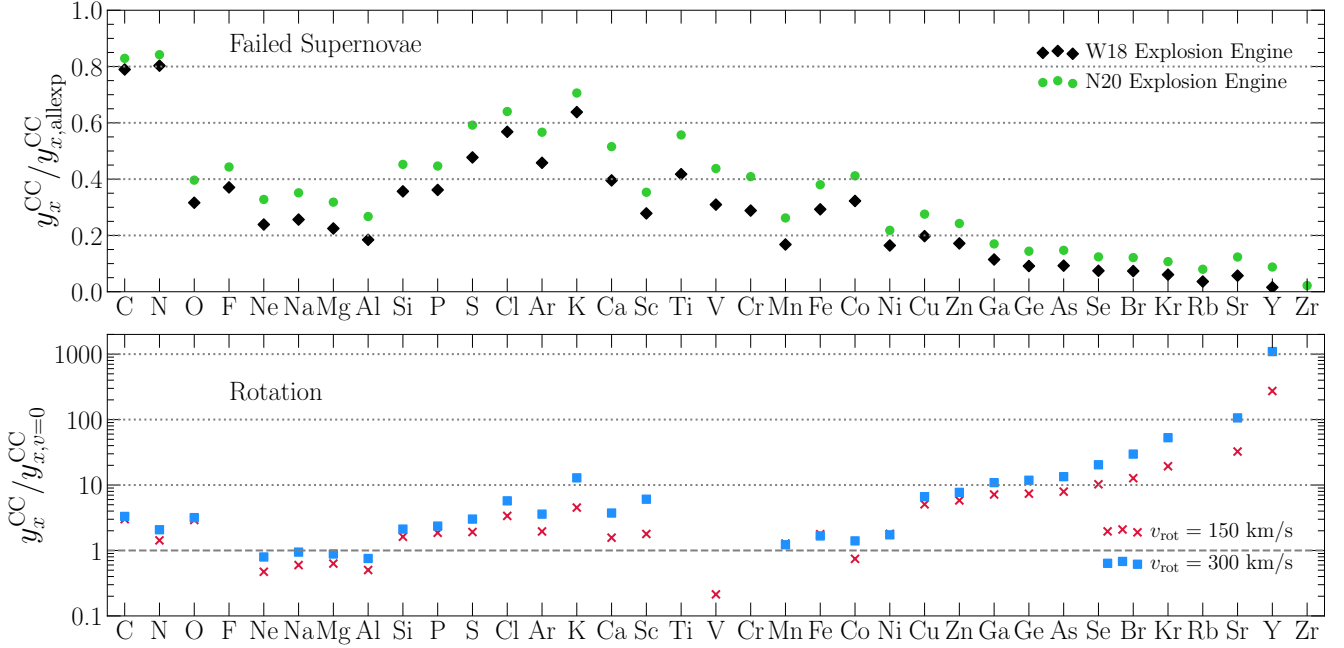


Figure 4. The effects of failed supernovae (top) and rotation (bottom) on population-averaged massive star yields, computed with `VICE`'s `vice.yields.ccsne.fractional` function using stellar model predictions available in the literature (see discussion in Section 5.1). **Top:** The yields of various elements under the W18 (black diamonds) and N20 (green circles) explosion mechanisms from Sukhbold et al. (2016), relative to the case where all massive stars explode as a CCSN at the ends of their lives (Griffith et al. 2021). **Bottom:** The yields of the same elements assuming initial rotational velocities of $v_{\text{rot}} = 150$ km/s (red 'x' marks) and $v_{\text{rot}} = 300$ km/s (blue squares), relative to the non-rotating case ($v_{\text{rot}} = 0$). **Summary:** Failed supernovae and rotation each individually introduce factor of a \gtrsim few uncertainties in the predicted yields of most metals, so an empirical benchmark would provide an important test for stellar models.

depletion dominates the scatter, then the true D/H of the ISM should correspond to the upper envelope of the distribution at $\gtrsim 2 \times 10^{-5}$ (Prodanović et al. 2010). Both scales of stellar yields are broadly consistent with this benchmark.

Figure 3 shows the three-way relationship between O/H, D/H, and $^3\text{He}/^4\text{He}$ in the present-day ISM. Each curve shows the corresponding pair of quantities in the ISM between $R = 3$ and 12 kpc. Currently, the Sun is the only system with a measurement in all three of these panels. The left panel shows that D/H and $^3\text{He}/^4\text{He}$ follow a tight relation regardless of the choice of ejection or radial flows. This outcome arises because deuterium burning leaves behind ^3He as a byproduct through the $d(p,\gamma)^3\text{He}$ reaction. The middle panel of Figure 3 indicates that ejection and radial gas flows lead to similar D/H–O/H relations. The normalization is most directly sensitive to the scale of stellar yields for the same reasons discussed above in the context of Figure 2. Weinberg (2017) found this connection between D/H and y/Z_{\odot} in one-zone models using ejection. Figure 3 indicates that our models are in excellent agreement with the D/H–O/H relation that they calculated, even with radial gas flows. van de Voort et al. (2018) found similar results in hydrodynamic simulations. The right panel of Figure 3 indicates that the $^3\text{He}/^4\text{He}$ ratio follows the same relationship with O/H as D/H. This three-way trend could be useful for sharpening the precision of measurements of

the primordial $^3\text{He}/^4\text{He}$ ratio (see discussion in Section 5.2 below).

5. DISCUSSION

5.1. The Scale of Stellar Yields

In this section, we highlight prior work showcasing the potential impact of determining the scale of stellar yields empirically. We compute population-averaged yields from massive stars for all elements between carbon and zirconium using tables of massive star models available in the literature. We use `VICE`'s `vice.yields.ccsne.fractional` function, which computes the yield according to

$$y_x^{\text{CC}} = \frac{\int_8^u (E(m)m_x + w_x - Z_x(m - m_{\text{rem}})) \frac{dN}{dm} dm}{\int_l^u m \frac{dN}{dm} dm}, \quad (4)$$

where m_x is the explosive yield of the element x from a star of initial mass m , $E(m)$ is the fraction of stars at that mass that explode, w_x is the yield of x that is released through stellar winds, and m_{rem} is the remnant mass. The corrective factor $Z_x(m - m_{\text{rem}})$ converts from a gross yield to a net yield by subtracting off the mass in the ejecta that was present when the stars formed. The denominator simply normalizes by the total mass of stars formed across the IMF.

The top panel of Figure 4 shows the effects of failed supernovae on the population-averaged yield, which affects $E(m)$ in Equation 4 above. We use the yields computed by Sukhbold et al. (2016), wherein the outcome of explosion or non-explosion is determined self-consistently through the neutrino mechanism. We focus on their “W18” and “N20” explosion models and normalize the yields by the results with $E(m) = 1$, which Griffith et al. (2021) computed by forcing explosions where the W18 model otherwise collapsed. The bottom panel of Figure 4 isolates the effects of massive star rotation by solving Equation 4 for stellar models with different initial angular momenta. We use the tables provided by Limongi & Chieffi (2018) at $v_{\text{rot}} = 150$ and 300 km/s, normalizing by the predictions with $v_{\text{rot}} = 0$.

Broadly, failed supernovae and rotation affect yields by factors of a \sim few for most elements. C and N are minimally affected by black hole formation, since a large portion of their yield emerges from massive star winds (see discussion in Griffith et al. 2021). For α -capture and iron-peak elements, failed supernovae reduce yields by factors of $\sim 2 - 3$. The effects of rotation are at a similar scale for these elements. Some elements (e.g., Ti, Cr, Rb) have negative net yields with $v_{\text{rot}} = 0$ but positive yields with $v_{\text{rot}} > 0$ and therefore do not show up in the bottom panel of Figure 4. For the heaviest elements shown here, which approach the first s-process peak at the Sr-Y-Zr group, rotation and failed supernovae effect yields by an order of magnitude or more. These effects underscore the notion that empirical benchmarks of the scale of stellar yields could be useful in pinning down uncertain processes, of which rotation and failed supernovae are only two examples (see discussion in Section 1).

5.2. The Primordial Helium Isotope Ratio

In this section, we demonstrate that mapping ${}^3\text{He}/{}^4\text{He}$ in the ISM across the MW would enable the first measurement of the primordial helium isotope ratio, $({}^3\text{He}/{}^4\text{He})_p$. To this end, we construct a mock sample of ${}^3\text{He}/{}^4\text{He}$ measurements using our ejection-driven GCE model with the $y/Z_{\odot} = 2$ yield scale. This model most clearly reproduces the observed trends in metallicity with stellar age across the Galactic disk (see discussion in Johnson et al. 2025 and Johnson 2025). We start with the present-day ISM composition at Galactocentric radii of $R = 5, 7, 9$, and 11 kpc. We randomly sample offsets from the predicted O abundances to mimic a measurement uncertainty of $\sigma([O/H]) = 0.02$, which is typical of modern high-resolution spectroscopic surveys (e.g., Buder et al. 2025; Mészáros et al. 2025). We use an uncertainty of $\sigma({}^3\text{He}/{}^4\text{He}) = 0.13$, which is the precision reached by Cooke et al. (2022) for the Orion Nebula. Measurements in more distant H II regions may carry higher uncertainties, but we use this fiducial value for this simple forecast.

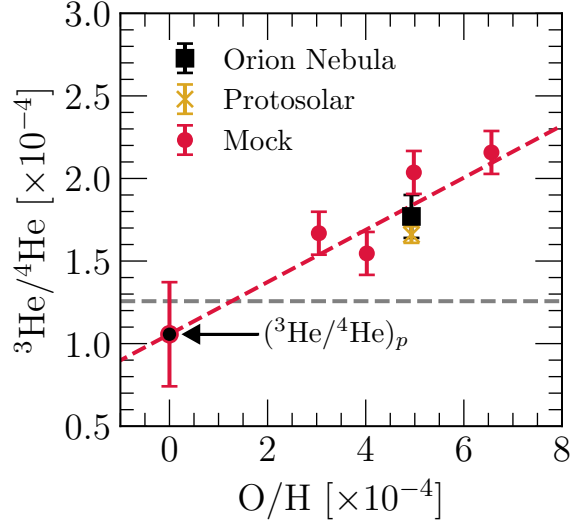


Figure 5. An inference of the primordial ${}^3\text{He}/{}^4\text{He}$ ratio, $({}^3\text{He}/{}^4\text{He})_p$, using available measurements from the literature combined with mock data from our GCE model using ejection with the $y/Z_{\odot} = 2$ yield scale (see discussion in Section 3). The black square and gold \times symbol indicate measurements of ${}^3\text{He}/{}^4\text{He}$ in the Orion Nebula by Cooke et al. (2022) and in Jupiter’s atmosphere by Mahaffy et al. (1998), respectively. Red circles show mock measurements drawn from the GCE model at the present day at Galactocentric radii of $R = 5, 7, 9$, and 11 kpc, offset by measurement uncertainties of $\sigma([O/H]) = 0.02$ and $\sigma({}^3\text{He}/{}^4\text{He}) = 0.13 \times 10^{-4}$ (see discussion in Section 5.2). The red dashed line shows the line of best-fit to these data, with the intercept at $O/H = 0$ marked as the inferred primordial isotope rate of $({}^3\text{He}/{}^4\text{He})_p = (1.06 \pm 0.32) \times 10^{-4}$. The grey dashed line marks the value of $({}^3\text{He}/{}^4\text{He})_p$ used as input to our GCE models. **Summary:** Measurements of the ${}^3\text{He}/{}^4\text{He}$ ratio along ~ 4 additional sightlines within distances of $\lesssim 3$ kpc, each achieving similar precision as Cooke et al. (2022), would provide a measurement of $({}^3\text{He}/{}^4\text{He})_p$ with $\sim 30\%$ precision.

Figure 5 shows the resulting mock sample alongside the existing measurements by Cooke et al. (2022) and in Jupiter’s atmosphere by Mahaffy et al. (1998). We assume solar O/H for the Orion Nebula, consistent with observations (D’Orazi et al. 2009). Following previous estimates of the primordial elemental abundance of He (e.g., Peimbert & Torres-Peimbert 1974; Izotov et al. 2014; Peimbert et al. 2016; Fernández et al. 2019; Valerdi & Peimbert 2019; Hsyu et al. 2020; Aver et al. 2021), the primordial isotope ratio can be determined by extrapolating this trend to $O/H = 0$. We perform a linear regression to these six data points, finding a slope of 0.158 ± 0.065 and an intercept of $({}^3\text{He}/{}^4\text{He})_p = (1.06 \pm 0.32) \times 10^{-4}$. These uncertainties correspond to $\sim 40\%$ precision of the slope of the trend and $\sim 30\%$ precision of the primordial helium isotope ratio. We explored variations in the random number seed used to draw the mock sample, finding uncertainties in $({}^3\text{He}/{}^4\text{He})_p$ ranging from $\sim 15\%$ to $\sim 40\%$ precision. We se-

lect this particular random subsample because it is typical but slightly conservative compared to other random draws. In general, measurements across a broad range of Galactocentric radii lead to a higher forecasted precision in $(^3\text{He}/^4\text{He})_p$. This outcome arises because sampling a range of Galactocentric radii also samples a range of metallicity due to the radial abundance gradient (see Figure 2). In detail, the $^3\text{He}/^4\text{He}$ -O/H relation is slightly non-linear, more noticeably so in the $y/Z_\odot = 1$ scale than $y/Z_\odot = 2$ (see Figure 3). The degree of non-linearity is subtle, so a linear relation should suffice for the foreseeable future, until the sample size and measurement precision of $^3\text{He}/^4\text{He}$ improve substantially.

5.3. Measurements

5.3.1. Helium

The most reliable method for measuring the helium isotope ratio of the ISM follows Cooke et al. (2022). This approach uses the light from a background star and measures the column density of helium in the metastable nuclear excited state, He I^* , in absorption due to a foreground screen of dense and highly ionized gas. Initially described in Cooke (2015), this method compares the line profiles of multiple He I^* transitions. In principle, differences in line profiles provide an unambiguous measurement of $^3\text{He}/^4\text{He}$ because the isotope shift is different for all He I^* transitions. The ionization potentials of ^3He and ^4He are also nearly identical, eliminating the need for an ionization correction. In Cooke et al. (2022), we used the transitions at $\lambda 3188$ Å, $\lambda 3889$ Å, and $\lambda 1.0833$ μm. The optical transitions have isotope shifts of only ~ 10 km/s, so their line profiles are dominated by $^4\text{He I}^*$. The $^3\text{He I}^*$ column density then follows from the $\lambda 1.0833$ μm line, where the isotope shift is ~ 35 km/s.

An important challenge with this approach is that metastable helium is rare. Historically, efforts to detect He I^* have often yielded upper limits (see discussion in Indriolo et al. 2009). Successful detections have been reported along sightlines toward hot stars in the Orion Nebula (Wilson 1937; O’Dell et al. 1993; Oudmaijer et al. 1997), in NGC 6611 (Evans et al. 2005), and toward ζ Ophiuchus (Galazutdinov & Krelowski 2012). Helium nuclei only exist in the metastable state when He^+ recaptures an electron that has the same spin as the one already present in the He^+ ion. Therefore, the observed absorption likely arises at the edge of the He II ionization region. Wolf-Rayets, blue supergiants, and O/B stars are therefore potentially useful targets, since they are hot enough to ionize He. Hot stars also have implicitly clean spectra near the He I^* transitions of interest. In red and yellow supergiants, carbon features appear near the 1.0833 μm line.

Ground state helium is unfortunately not useful for measuring the isotope ratio. Available measurements in the radio (Balser & Bania 2018, see Figure 2 and discussion in Sec-

tion 4) do not reach sufficient precision for these purposes. All other helium transitions are in the far-UV, which would require observatories in space and sightlines that are not attenuated by H I absorption in the same gas cloud (see, e.g., Cooke & Fumagalli 2018). However, the isotope shifts in the UV are small, of order ~ 12 km/s. The $\lambda 1.0833$ μm line has the largest isotope shift (~ 35 km/s) of all helium transitions. Therefore, for the foreseeable future, the best path toward measuring the Galactic distribution of $^3\text{He}/^4\text{He}$ is through the metastable transitions along sightlines toward massive stars.

5.3.2. Deuterium

D/H is most often measured using Lyman series transitions (e.g., Rogerson & York 1973; Adams 1976). Historically, D/H measurements have been made along sightlines toward stars near the Sun (e.g., Linsky et al. 2006 and references therein) and toward high-redshift quasars or damped Lyman- α systems (see, e.g., the review by Cooke 2026). The former provide measurements of D/H in the local ISM that we have used in this paper (see Figure 2), while the latter have been used to infer the primordial D/H ratio (e.g., Cooke et al. 2018; Kislysyn et al. 2024). With an isotope shift of ~ 82 km/s in Lyman series transitions, D I and H I can be reliably distinguished from one another with spectral resolution of $R \gtrsim 25,000$. D/H measurements therefore do not face the same technical challenges as $^3\text{He}/^4\text{He}$ measurements (see discussion in Section 5.3.1 above). However, the Lyman series is sufficiently far into the ultraviolet (UV) that MW measurements require a space-based UV-sensitive echelle spectrograph. The usefulness of mapping D/H across the MW points to a need for continued investment in UV-sensitive facilities in space.

6. CONCLUSIONS

Building on previous GCE models, we have demonstrated that metal abundances in the MW disk are subject to a “source-sink” degeneracy. Yields of all metals from stars can be uniformly increased, but similar metallicities arise as long as one proportionally ejects more gas from the ISM (Hartwick 1976; Cooke et al. 2022; Johnson et al. 2023c; Sandford et al. 2024). In this paper, we have shown that radial gas flows (e.g., Lacey & Fall 1985; Bilitewski & Schönrich 2012; Johnson 2025) have qualitatively similar effects. High stellar yields result in similar metal abundances as lower yields if the inward flow velocity is proportionally faster (see Figure 1).

This yield-ejection-velocity degeneracy can be broken by mapping the $^3\text{He}/^4\text{He}$ or D/H isotope ratios in the ISM across the MW disk (see Figure 2). Non-metals have different production and destruction channels than metals. By tracing different processes, measurements of hydrogen and helium isotopes can break this degeneracy. Our models predict similar radial profiles in both $^3\text{He}/^4\text{He}$ and D/H when swapping ejection for radial gas flows, indicating that this connection

is independent of the assumed set of GCE parameters. Non-metal isotope ratios are therefore useful empirical diagnostics of the scale of stellar yields, in line with prior work (e.g., Weinberg 2017; Cooke et al. 2022).

Breaking this degeneracy would provide a useful benchmark for stellar evolution models. Poorly understood processes introduce uncertainties in metal yields at the factor of a \gtrsim few level for most elements (see Figure 4 and discussion in Section 5.1). We have highlighted this result for failed supernovae (Griffith et al. 2021) and rotation (Limongi & Chieffi 2018, see Figure 4), but similar uncertainties are introduced by mass loss (e.g., Sukhbold et al. 2016), convection (e.g., Chieffi et al. 2001), and nuclear reaction rates (e.g., Herwig & Austin 2004). Precise empirical constraints on the total metal yield from stellar populations would allow stellar evolution and supernova models to be ruled out based on over- or under-production of certain elements. Given dust depletion of D/H in the ISM (Linsky et al. 2006), $^3\text{He}/^4\text{He}$ might be a better tracer of the effects discussed by Weinberg (2017). For example, measurements of $^3\text{He}/^4\text{He}$ may allow us to test if the MW disk exhibits large metallicity variations due to accretion of low-metallicity gas (e.g., De Cia et al. 2021). If $^3\text{He}/^4\text{He}$ varies smoothly across the Galactic disk, that result would confirm the long-standing suggestions that the low D/H along some sightlines arises due to dust depletion.

Mapping $^3\text{He}/^4\text{He}$ across the Galactic disk would also enable the first inference of the primordial helium isotope ratio, $(^3\text{He}/^4\text{He})_p$ (see Figure 5). With four additional $^3\text{He}/^4\text{He}$ measurements within ~ 3 kpc of the Sun, we project a $\sim 30\%$ statistical uncertainty in $(^3\text{He}/^4\text{He})_p$. This primordial helium isotope ratio would provide a yet unachieved test of current models of BBN (see discussion in Cooke et al. 2022). The relationship between D/H, O/H, and $^3\text{He}/^4\text{He}$ could also

be of potential use in pinning down the composition of the primordial Universe more precisely (see Figure 3).

Ultimately, the yield-ejection-velocity degeneracy underscores the notion that metal abundances alone are fundamentally limited in their information content. Specifically, metal production on its own does not specify the metallicity scale. Metallicity is also influenced by the amount of hydrogen that newly produced metals mix with. Unsurprisingly, this information is encoded in the relative numbers of hydrogen isotopes. Breaking this degeneracy provides information on the timescales of metallicity growth in galaxies, which is sensitive to the relative balance of accretion, star formation, and ejection (see discussion in, e.g., Johnson et al. 2025). These processes are central components of galaxy evolution models. Each method of breaking the degeneracy carries its own challenges and sources of systematic uncertainty (see discussion in Section 1). Although the measurements are challenging (see discussion in Section 5.3), a detailed inventory of non-metals would provide constraints useful for a range of purposes in astrophysics. Currently, there are only a handful of available measurements along sightlines in the MW (see discussion in Section 2). Even small additions to the current sample would significantly improve the landscape.

ACKNOWLEDGEMENTS

We are grateful to David Weinberg for valuable discussion of this project. JWJ acknowledges support from a Carnegie Theoretical Astrophysics Center postdoctoral fellowship. During this work, RJC was supported by a Royal Society University Research Fellowship. RJC acknowledges support from STFC (ST/X001075/1). This research has made use of NASA’s Astrophysics Data System.

REFERENCES

Adams, T. F. 1976, A&A, 50, 461

Alpher, R. A., Bethe, H., & Gamow, G. 1948, Physical Review, 73, 803, doi: [10.1103/PhysRev.73.803](https://doi.org/10.1103/PhysRev.73.803)

Asplund, M., Grevesse, N., Sauval, A. J., & Scott, P. 2009, ARA&A, 47, 481, doi: [10.1146/annurev.astro.46.060407.145222](https://doi.org/10.1146/annurev.astro.46.060407.145222)

Aver, E., Berg, D. A., Olive, K. A., et al. 2021, JCAP, 2021, 027, doi: [10.1088/1475-7516/2021/03/027](https://doi.org/10.1088/1475-7516/2021/03/027)

Balser, D. S., & Bania, T. M. 2018, AJ, 156, 280, doi: [10.3847/1538-3881/aaeb2b](https://doi.org/10.3847/1538-3881/aaeb2b)

Bilitewski, T., & Schönrich, R. 2012, MNRAS, 426, 2266, doi: [10.1111/j.1365-2966.2012.21827.x](https://doi.org/10.1111/j.1365-2966.2012.21827.x)

Bird, J. C., Kazantzidis, S., Weinberg, D. H., et al. 2013, ApJ, 773, 43, doi: [10.1088/0004-637X/773/1/43](https://doi.org/10.1088/0004-637X/773/1/43)

Bodenheimer, P. 1966, ApJ, 144, 103, doi: [10.1086/148592](https://doi.org/10.1086/148592)

Buder, S., Kos, J., Wang, X. E., et al. 2025, PASA, 42, e051, doi: [10.1017/pasa.2025.26](https://doi.org/10.1017/pasa.2025.26)

Chaplin, W. J., & Miglio, A. 2013, ARA&A, 51, 353, doi: [10.1146/annurev-astro-082812-140938](https://doi.org/10.1146/annurev-astro-082812-140938)

Chieffi, A., Domínguez, I., Limongi, M., & Straniero, O. 2001, ApJ, 554, 1159, doi: [10.1086/321387](https://doi.org/10.1086/321387)

Cooke, R. 2024, arXiv e-prints, arXiv:2409.06015, doi: [10.48550/arXiv.2409.06015](https://doi.org/10.48550/arXiv.2409.06015)

Cooke, R. 2026, in Encyclopedia of Astrophysics, Vol. 5, 159–183, doi: [10.1016/B978-0-443-21439-4.00046-8](https://doi.org/10.1016/B978-0-443-21439-4.00046-8)

Cooke, R. J. 2015, ApJL, 812, L12, doi: [10.1088/2041-8205/812/1/L12](https://doi.org/10.1088/2041-8205/812/1/L12)

Cooke, R. J., & Fumagalli, M. 2018, Nature Astronomy, 2, 957, doi: [10.1038/s41550-018-0584-z](https://doi.org/10.1038/s41550-018-0584-z)

Cooke, R. J., Noterdaeme, P., Johnson, J. W., et al. 2022, ApJ, 932, 60, doi: [10.3847/1538-4357/ac6503](https://doi.org/10.3847/1538-4357/ac6503)

Cooke, R. J., Pettini, M., & Steidel, C. C. 2018, ApJ, 855, 102, doi: [10.3847/1538-4357/aaab53](https://doi.org/10.3847/1538-4357/aaab53)

Cooper, T. J., Rudie, G. C., Chen, H.-W., et al. 2021, MNRAS, 508, 4359, doi: [10.1093/mnras/stab2869](https://doi.org/10.1093/mnras/stab2869)

da Silva, R., D’Orazi, V., Palla, M., et al. 2023, A&A, 678, A195, doi: [10.1051/0004-6361/202346982](https://doi.org/10.1051/0004-6361/202346982)

De Cia, A., Jenkins, E. B., Fox, A. J., et al. 2021, Nature, 597, 206, doi: [10.1038/s41586-021-03780-0](https://doi.org/10.1038/s41586-021-03780-0)

D’Orazi, V., Randich, S., Flaccomio, E., et al. 2009, A&A, 501, 973, doi: [10.1051/0004-6361/200811241](https://doi.org/10.1051/0004-6361/200811241)

Ertl, T., Janka, H. T., Woosley, S. E., Sukhbold, T., & Ugliano, M. 2016, ApJ, 818, 124, doi: [10.3847/0004-637X/818/2/124](https://doi.org/10.3847/0004-637X/818/2/124)

Evans, C. J., Smartt, S. J., Lee, J. K., et al. 2005, A&A, 437, 467, doi: [10.1051/0004-6361:20042446](https://doi.org/10.1051/0004-6361:20042446)

Fernández, V., Terlevich, E., Díaz, A. I., & Terlevich, R. 2019, MNRAS, 487, 3221, doi: [10.1093/mnras/stz1433](https://doi.org/10.1093/mnras/stz1433)

Gaia Collaboration, Brown, A. G. A., Vallenari, A., et al. 2021, A&A, 649, A1, doi: [10.1051/0004-6361/202039657](https://doi.org/10.1051/0004-6361/202039657)

Galazutdinov, G. A., & Krelowski, J. 2012, MNRAS, 422, 3457, doi: [10.1111/j.1365-2966.2012.20856.x](https://doi.org/10.1111/j.1365-2966.2012.20856.x)

Gallart, C., Surot, F., Cassisi, S., et al. 2024, arXiv e-prints, arXiv:2402.09399, doi: [10.48550/arXiv.2402.09399](https://doi.org/10.48550/arXiv.2402.09399)

Gallazzi, A., Brinchmann, J., Charlot, S., & White, S. D. M. 2008, MNRAS, 383, 1439, doi: [10.1111/j.1365-2966.2007.12632.x](https://doi.org/10.1111/j.1365-2966.2007.12632.x)

Gandhi, P. J., Wetzel, A., Hopkins, P. F., et al. 2022, MNRAS, 516, 1941, doi: [10.1093/mnras/stac2228](https://doi.org/10.1093/mnras/stac2228)

GRAVITY Collaboration, Abuter, R., Amorim, A., et al. 2019, A&A, 625, L10, doi: [10.1051/0004-6361/201935655](https://doi.org/10.1051/0004-6361/201935655)

Griffith, E. J., Sukhbold, T., Weinberg, D. H., et al. 2021, ApJ, 921, 73, doi: [10.3847/1538-4357/ac1bac](https://doi.org/10.3847/1538-4357/ac1bac)

Griffith, E. J., Weinberg, D. H., Buder, S., et al. 2022, ApJ, 931, 23, doi: [10.3847/1538-4357/ac5826](https://doi.org/10.3847/1538-4357/ac5826)

Haislmaier, K. J., Tripp, T. M., Katz, N., et al. 2021, MNRAS, 502, 4993, doi: [10.1093/mnras/staa3544](https://doi.org/10.1093/mnras/staa3544)

Hartwick, F. D. A. 1976, ApJ, 209, 418, doi: [10.1086/154735](https://doi.org/10.1086/154735)

Hegedűs, V., Mészáros, S., Jofré, P., et al. 2023, A&A, 670, A107, doi: [10.1051/0004-6361/202244813](https://doi.org/10.1051/0004-6361/202244813)

Herwig, F. 2005, ARA&A, 43, 435, doi: [10.1146/annurev.astro.43.072103.150600](https://doi.org/10.1146/annurev.astro.43.072103.150600)

Herwig, F., & Austin, S. M. 2004, ApJL, 613, L73, doi: [10.1086/424872](https://doi.org/10.1086/424872)

Hoyle, F., & Tayler, R. J. 1964, Nature, 203, 1108, doi: [10.1038/2031108a0](https://doi.org/10.1038/2031108a0)

Hsyu, T., Cooke, R. J., Prochaska, J. X., & Bolte, M. 2020, ApJ, 896, 77, doi: [10.3847/1538-4357/ab91af](https://doi.org/10.3847/1538-4357/ab91af)

Hurley, J. R., Pols, O. R., & Tout, C. A. 2000, MNRAS, 315, 543, doi: [10.1046/j.1365-8711.2000.03426.x](https://doi.org/10.1046/j.1365-8711.2000.03426.x)

Indriolo, N., Hobbs, L. M., Hinkle, K. H., & McCall, B. J. 2009, ApJ, 703, 2131, doi: [10.1088/0004-637X/703/2/2131](https://doi.org/10.1088/0004-637X/703/2/2131)

Izotov, Y. I., Thuan, T. X., & Guseva, N. G. 2014, MNRAS, 445, 778, doi: [10.1093/mnras/stu1771](https://doi.org/10.1093/mnras/stu1771)

Johnson, J. W. 2025, arXiv e-prints, arXiv:2510.05223. <https://arxiv.org/abs/2510.05223>

Johnson, J. W., Kochanek, C. S., & Stanek, K. Z. 2023a, MNRAS, 526, 5911, doi: [10.1093/mnras/stad3019](https://doi.org/10.1093/mnras/stad3019)

Johnson, J. W., & Weinberg, D. H. 2020, MNRAS, 498, 1364, doi: [10.1093/mnras/staa2431](https://doi.org/10.1093/mnras/staa2431)

Johnson, J. W., Weinberg, D. H., Vincenzo, F., Bird, J. C., & Griffith, E. J. 2023b, MNRAS, 520, 782, doi: [10.1093/mnras/stad057](https://doi.org/10.1093/mnras/stad057)

Johnson, J. W., Weinberg, D. H., Vincenzo, F., et al. 2021, MNRAS, 508, 4484, doi: [10.1093/mnras/stab2718](https://doi.org/10.1093/mnras/stab2718)

Johnson, J. W., Conroy, C., Johnson, B. D., et al. 2023c, MNRAS, 526, 5084, doi: [10.1093/mnras/stad2985](https://doi.org/10.1093/mnras/stad2985)

Johnson, J. W., Weinberg, D. H., Blanc, G. A., et al. 2025, ApJ, 988, 8, doi: [10.3847/1538-4357/addrbe5](https://doi.org/10.3847/1538-4357/addrbe5)

Kennicutt, Robert C., J. 1998, ApJ, 498, 541, doi: [10.1086/305588](https://doi.org/10.1086/305588)

Kewley, L. J., Nicholls, D. C., & Sutherland, R. S. 2019, ARA&A, 57, 511, doi: [10.1146/annurev-astro-081817-051832](https://doi.org/10.1146/annurev-astro-081817-051832)

Kislitsyn, P. A., Balashev, S. A., Murphy, M. T., et al. 2024, MNRAS, 528, 4068, doi: [10.1093/mnras/stae248](https://doi.org/10.1093/mnras/stae248)

Kotar, E., Ota, S., Dewey, A., et al. 2025, arXiv e-prints, arXiv:2509.19583. <https://arxiv.org/abs/2509.19583>

Kroupa, P. 2001, MNRAS, 322, 231, doi: [10.1046/j.1365-8711.2001.04022.x](https://doi.org/10.1046/j.1365-8711.2001.04022.x)

Kumar, S., Chen, H.-W., Qu, Z., et al. 2024, arXiv e-prints, arXiv:2408.15824, doi: [10.48550/arXiv.2408.15824](https://doi.org/10.48550/arXiv.2408.15824)

Lacey, C. G., & Fall, S. M. 1985, ApJ, 290, 154, doi: [10.1086/162970](https://doi.org/10.1086/162970)

Lagarde, N., Charbonnel, C., Decressin, T., & Hagelberg, J. 2011, A&A, 536, A28, doi: [10.1051/0004-6361/201117739](https://doi.org/10.1051/0004-6361/201117739)

Lagarde, N., Romano, D., Charbonnel, C., et al. 2012, A&A, 542, A62, doi: [10.1051/0004-6361/201219132](https://doi.org/10.1051/0004-6361/201219132)

Larson, R. B. 1972, Nature Physical Science, 236, 7, doi: [10.1038/physci236007a0](https://doi.org/10.1038/physci236007a0)

—. 1974, MNRAS, 166, 585, doi: [10.1093/mnras/166.3.585](https://doi.org/10.1093/mnras/166.3.585)

Limongi, M., & Chieffi, A. 2018, ApJS, 237, 13, doi: [10.3847/1538-4365/aacb24](https://doi.org/10.3847/1538-4365/aacb24)

Linsky, J. L., Draine, B. T., Moos, H. W., et al. 2006, ApJ, 647, 1106, doi: [10.1086/505556](https://doi.org/10.1086/505556)

Maeder, A., & Meynet, G. 1989, A&A, 210, 155

Magg, E., Bergemann, M., Serenelli, A., et al. 2022, A&A, 661, A140, doi: [10.1051/0004-6361/202142971](https://doi.org/10.1051/0004-6361/202142971)

Mahaffy, P. R., Donahue, T. M., Atreya, S. K., Owen, T. C., & Niemann, H. B. 1998, SSRv, 84, 251

Majewski, S. R., Schiavon, R. P., Frinchaboy, P. M., et al. 2017, AJ, 154, 94, doi: [10.3847/1538-3881/aa784d](https://doi.org/10.3847/1538-3881/aa784d)

Matteucci, F. 2021, A&A Rv, 29, 5, doi: [10.1007/s00159-021-00133-8](https://doi.org/10.1007/s00159-021-00133-8)

Mazzitelli, I., & Moretti, M. 1980, ApJ, 235, 955, doi: [10.1086/157700](https://doi.org/10.1086/157700)

Mészáros, S., Jofré, P., Johnson, J. A., et al. 2025, AJ, 170, 96, doi: [10.3847/1538-3881/ade4b9](https://doi.org/10.3847/1538-3881/ade4b9)

Niemann, H. B., Harpold, D. N., Atreya, S. K., et al. 1992, SSRv, 60, 111, doi: [10.1007/BF00216852](https://doi.org/10.1007/BF00216852)

O'Dell, C. R., Valk, J. H., Wen, Z., & Meyer, D. M. 1993, ApJ, 403, 678, doi: [10.1086/172238](https://doi.org/10.1086/172238)

Oudmaijer, R. D., Drew, J. E., Barlow, M. J., Crawford, I. A., & Proga, D. 1997, MNRAS, 291, 110, doi: [10.1093/mnras/291.1.110](https://doi.org/10.1093/mnras/291.1.110)

Padovani, P., & Matteucci, F. 1993, ApJ, 416, 26, doi: [10.1086/173212](https://doi.org/10.1086/173212)

Peebles, P. J. E. 1966, ApJ, 146, 542, doi: [10.1086/148918](https://doi.org/10.1086/148918)

Peeples, M. S., Werk, J. K., Tumlinson, J., et al. 2014, ApJ, 786, 54, doi: [10.1088/0004-637X/786/1/54](https://doi.org/10.1088/0004-637X/786/1/54)

Peimbert, A., Peimbert, M., & Luridiana, V. 2016, RMxAA, 52, 419, doi: [10.48550/arXiv.1608.02062](https://doi.org/10.48550/arXiv.1608.02062)

Peimbert, M., & Torres-Peimbert, S. 1974, ApJ, 193, 327, doi: [10.1086/153166](https://doi.org/10.1086/153166)

Pejcha, O., & Thompson, T. A. 2015, ApJ, 801, 90, doi: [10.1088/0004-637X/801/2/90](https://doi.org/10.1088/0004-637X/801/2/90)

Péroux, C., & Howk, J. C. 2020, ARA&A, 58, 363, doi: [10.1146/annurev-astro-021820-120014](https://doi.org/10.1146/annurev-astro-021820-120014)

Pessi, T., Anderson, J. P., Lyman, J. D., et al. 2023, ApJL, 955, L29, doi: [10.3847/2041-8213/acf7c6](https://doi.org/10.3847/2041-8213/acf7c6)

Pezzulli, G., & Fraternali, F. 2016, MNRAS, 455, 2308, doi: [10.1093/mnras/stv2397](https://doi.org/10.1093/mnras/stv2397)

Pitrou, C., Coc, A., Uzan, J.-P., & Vangioni, E. 2021, MNRAS, 502, 2474, doi: [10.1093/mnras/stab135](https://doi.org/10.1093/mnras/stab135)

Portinari, L., & Chiosi, C. 2000, A&A, 355, 929, doi: [10.48550/arXiv.astro-ph/0002145](https://doi.org/10.48550/arXiv.astro-ph/0002145)

Prochaska, J. X., Gawiser, E., Wolfe, A. M., Castro, S., & Djorgovski, S. G. 2003, ApJL, 595, L9, doi: [10.1086/378945](https://doi.org/10.1086/378945)

Prodanović, T., Steigman, G., & Fields, B. D. 2010, MNRAS, 406, 1108, doi: [10.1111/j.1365-2966.2010.16734.x](https://doi.org/10.1111/j.1365-2966.2010.16734.x)

Roberts, J. D., Pinsonneault, M. H., Johnson, J. A., Dubay, L. O., & Johnson, J. W. 2025, arXiv e-prints, arXiv:2509.25321, doi: [10.48550/arXiv.2509.25321](https://doi.org/10.48550/arXiv.2509.25321)

Rodríguez, Ó., Maoz, D., & Nakar, E. 2023, ApJ, 955, 71, doi: [10.3847/1538-4357/ace2bd](https://doi.org/10.3847/1538-4357/ace2bd)

Rogerson, J. B., & York, D. G. 1973, ApJL, 186, L95, doi: [10.1086/181366](https://doi.org/10.1086/181366)

Sameer, Charlton, J. C., Wakker, B. P., et al. 2024, MNRAS, 530, 3827, doi: [10.1093/mnras/stae962](https://doi.org/10.1093/mnras/stae962)

Sandford, N. R., Weinberg, D. H., Weisz, D. R., & Fu, S. W. 2024, MNRAS, 530, 2315, doi: [10.1093/mnras/stae1010](https://doi.org/10.1093/mnras/stae1010)

Schmidt, M. 1959, ApJ, 129, 243, doi: [10.1086/146614](https://doi.org/10.1086/146614)

—. 1963, ApJ, 137, 758, doi: [10.1086/147553](https://doi.org/10.1086/147553)

Schramm, D. N., & Turner, M. S. 1998, Reviews of Modern Physics, 70, 303, doi: [10.1103/RevModPhys.70.303](https://doi.org/10.1103/RevModPhys.70.303)

Sit, T., Weinberg, D. H., & Griffith, E. J. 2025, arXiv e-prints, arXiv:2503.07738, doi: [10.48550/arXiv.2503.07738](https://doi.org/10.48550/arXiv.2503.07738)

Soderblom, D. R. 2010, ARA&A, 48, 581, doi: [10.1146/annurev-astro-081309-130806](https://doi.org/10.1146/annurev-astro-081309-130806)

Spina, L., Magrini, L., & Cunha, K. 2022, Universe, 8, 87, doi: [10.3390/universe8020087](https://doi.org/10.3390/universe8020087)

Spitoni, E., & Matteucci, F. 2011, A&A, 531, A72, doi: [10.1051/0004-6361/201015749](https://doi.org/10.1051/0004-6361/201015749)

Steigman, G. 2007, Annual Review of Nuclear and Particle Science, 57, 463, doi: [10.1146/annurev.nucl.56.080805.140437](https://doi.org/10.1146/annurev.nucl.56.080805.140437)

Sukhbold, T., Ertl, T., Woosley, S. E., Brown, J. M., & Janka, H. T. 2016, ApJ, 821, 38, doi: [10.3847/0004-637X/821/1/38](https://doi.org/10.3847/0004-637X/821/1/38)

Thompson, T. A., & Heckman, T. M. 2024, ARA&A, 62, 529, doi: [10.1146/annurev-astro-041224-011924](https://doi.org/10.1146/annurev-astro-041224-011924)

Tinsley, B. M. 1980, FCPh, 5, 287, doi: [10.48550/arXiv.2203.02041](https://doi.org/10.48550/arXiv.2203.02041)

Tumlinson, J., Peebles, M. S., & Werk, J. K. 2017, ARA&A, 55, 389, doi: [10.1146/annurev-astro-091916-055240](https://doi.org/10.1146/annurev-astro-091916-055240)

Valerdi, M., & Peimbert, A. 2019, arXiv e-prints, arXiv:1905.05102, doi: [10.48550/arXiv.1905.05102](https://doi.org/10.48550/arXiv.1905.05102)

van de Voort, F., Quataert, E., Faucher-Giguère, C.-A., et al. 2018, MNRAS, 477, 80, doi: [10.1093/mnras/sty591](https://doi.org/10.1093/mnras/sty591)

Veilleux, S., Maiolino, R., Bolatto, A. D., & Aalto, S. 2020, A&A Rev, 28, 2, doi: [10.1007/s00159-019-0121-9](https://doi.org/10.1007/s00159-019-0121-9)

Ventura, P., Di Criscienzo, M., Carini, R., & D'Antona, F. 2013, MNRAS, 431, 3642, doi: [10.1093/mnras/stt444](https://doi.org/10.1093/mnras/stt444)

Wagoner, R. V., Fowler, W. A., & Hoyle, F. 1967, ApJ, 148, 3, doi: [10.1086/149126](https://doi.org/10.1086/149126)

Weinberg, D. H. 2017, ApJ, 851, 25, doi: [10.3847/1538-4357/aa96b2](https://doi.org/10.3847/1538-4357/aa96b2)

Weinberg, D. H., Andrews, B. H., & Freudenburg, J. 2017, ApJ, 837, 183, doi: [10.3847/1538-4357/837/2/183](https://doi.org/10.3847/1538-4357/837/2/183)

Weinberg, D. H., Griffith, E. J., Johnson, J. W., & Thompson, T. A. 2024, ApJ, 973, 122, doi: [10.3847/1538-4357/ad6313](https://doi.org/10.3847/1538-4357/ad6313)

Weller, M. K., Weinberg, D. H., & Johnson, J. W. 2025, MNRAS, 538, 1517, doi: [10.1093/mnras/staf373](https://doi.org/10.1093/mnras/staf373)

Willett, E., Miglio, A., Mackereth, J. T., et al. 2023, MNRAS, 526, 2141, doi: [10.1093/mnras/stad2374](https://doi.org/10.1093/mnras/stad2374)

Wilson, O. C. 1937, PASP, 49, 338, doi: [10.1086/124868](https://doi.org/10.1086/124868)

Yasui, C., Kobayashi, N., Saito, M., Izumi, N., & Ikeda, Y. 2023, ApJ, 943, 137, doi: [10.3847/1538-4357/ac94d5](https://doi.org/10.3847/1538-4357/ac94d5)

Zahedy, F. S., Chen, H.-W., Johnson, S. D., et al. 2019, MNRAS, 484, 2257, doi: [10.1093/mnras/sty3482](https://doi.org/10.1093/mnras/sty3482)

Zahedy, F. S., Chen, H.-W., Cooper, T. M., et al. 2021, MNRAS, 506, 877, doi: [10.1093/mnras/stab1661](https://doi.org/10.1093/mnras/stab1661)